Probing the dichotomy of square planar d^{10} complexes: Geometric and Electronic Structure of Nickel π-complexes

Addison N. Desnoyer,[†] Weiying He,[†] Shirin Behyan, Weiling Chiu, Jennifer A. Love,* and Pierre Kennepohl*

Ni π-complexes are widely postulated as intermediates in organometallic chemistry. However, the nature of the bonding in such complexes has not been extensively studied. Herein, we probe the geometric and electronic structure of a series of nickel π-complexes, Ni(dtbpe)(X) (dtbpe = di-*tert*butylphosphinoethane; X = alkene and carbonyl containing π-ligands), using a combination of ^{31}P NMR, Ni K-edge XAS, Ni K_β XES, and supporting density-functional computations. We observe that these complexes are best described as square planar d^{10} complexes with π-backbonding acting as the dominant factor in the M-L bond to the π ligand. The degree of backbonding correlates with both $^2J_{PP}$ and the energy of the clearly observable Ni 1s→4p_z pre-edge transition in the Ni K-edge XAS data, and is determined by the energy of the π^*_{ip} ligand acceptor orbital: unactivated olefinic ligands tend to be poor π-acids whereas ketones, aldehydes, and esters allow for greater backbonding. The strength of the backbonding from the neutral Ni(dtbpe) molecular fragment is dramatically increased *via* σ donation from the diphosphine ligands. In fact, backbonding is dominated by charge donation from the phosphines, which allows for strong backdonation even though the metal centre retains a formal d^{10} electronic configuration. We describe this interaction as a formal 3-centre-4-electron (3c-4e) interaction where the nickel centre mediates charge transfer from the phosphine σ-donors to the π^*_{ip} ligand acceptor orbital. The implications of this unusual bonding motif are described with respect to both geometric structure and reactivity.

Introduction

Over the last two decades, renewed interest in the redox non-innocence of ligands has led to their proliferation in inorganic chemistry.[1,2] In particular, the use of these ligands as electron reservoirs enables two-electron processes from first-row transition metal complexes, which typically exhibit single-electron chemistry.[3] In a pioneering example, Chirik and co-workers demonstrated that (PDI)Fe(N_2)$_2$ (PDI = 2,6-(2,6-^{i}Pr$_2$C$_6$H$_3$NCR)$_2$C$_5$H$_3$N, R = Me or Ph) catalyzes the formal [2+2] cyclization of diolefins to form cyclobutane rings.[4] Notably, the iron centre stays in the Fe(II) oxidation state throughout the catalytic cycle, with the PDI ligand acting as a two-electron reservoir. More recently, the Tsurugi, Arnold, and Mashima groups reported that both the geometric and electronic non-innocence of α-diimine ligands plays a key role in niobium-catalyzed chlorination of olefins, where the metal centre stays in the Nb(V) oxidation state and redox events occur on the diimine ligand.[5]

In contrast to these open-shell systems, closed-shell systems that rely on the ligand accepting and/or donating electron pairs are less common. A milestone example of this type of reactivity is the zirconium system reported by Heyduk, which allows for formal "oxidative addition" reactions to occur at a Zr(IV), d^0 metal centre.[6] In another example, we have recently shown that the oxidation of (TPA)Rh olefin complexes (TPA = tris(2-pyridylmethyl)amine) with H_2O_2 to form 2-rhodaoxetanes[7] is more accurately described as a ligand-centred oxidation,[8] rather than a metal-centred oxidation.[9] In this case, the π-ligand acts as a two-electron redox centre.

We have recently become interested in exploring the fundamental organometallic chemistry of earth-abundant, first-row transition metals. For example, we are exploring the organometallic chemistry of nickel,[10–13] which has undergone a renaissance in recent years.[14–20] Our focus has been the structure and reactivity of nickel π-complexes, which have been reported in a wide range of catalytic processes, including the catalytic coupling of CO_2 and ethylene,[5,21,30,31,22–29] intermolecular Tischenko coupling,[32–34] benzoxasilole synthesis,[35,36] aldol reaction,[37] allylic alkylation,[38] allylic amination,[39] allylic amidation,[40] epoxide functionalization,[41] and Suzuki-Miyaura coupling.[42] In addition, nickel π-complexes of heteroarenes have been identified as key intermediates in nickel-catalyzed catalyst transfer polycondensation to form polythiophenes.[43,44,53–55,45–52] Given the importance of nickel π-complexes, detailed exploration of their structure and reactivity is needed. Herein we report surprising aspects of the electronic

Department of Chemistry, The University of British Columbia, Vancouver, Canada.
† These authors contributed equally to this work.

structure and bonding in a series of nickel π-complexes relevant to catalysis.

		τ_4	$\Sigma\measuredangle_{Ni}$	$\Sigma\measuredangle_C$	r_{CO} (pm)	$J_{P,P}$ (Hz)
1	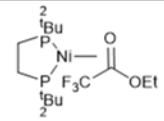	0.37	360.1°	341.7°	131.7	63
2	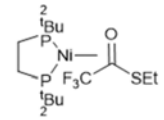	0.39	359.8°	345.4°	134.7	48
3	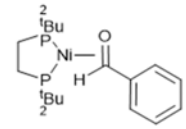	0.37	360.3°	351.7°	133.4	71
4	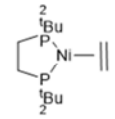	0.36	360.1°	352.6° 353.3°	141.9	-
5	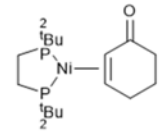	0.39	359.2°	352.3° 348.3°	141.6	61
6	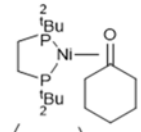	0.36	360.0°	344.7°	135.4	79
7	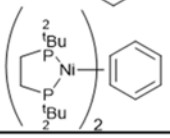	0.38	360.4°	355.4° 357.1°	142.1	-
	average	0.37	360.0°	350.3°	137.3	64

Chart 1 List of π complexes considered in this study identified by their compound number (bold), τ_4 value, sums of the angles about the metal centre ($\sum\measuredangle_{Ni}$) and carbons in the π ligand ($\sum\measuredangle_C$), C=X bond distance of the π ligand (r_{CX}), and NMR P,P coupling constants (J_{PP}).

In previous work, we noted that the $^{31}P\{^1H\}$ NMR spectroscopic data of a number of nickel π-complexes were consistent with typical d^{10} Ni(0) complexes (Chart 1).[10,11,56] In contrast, we also noted that the distorted square planar geometry with significant elongation of the π-bond were more consistent with a d^8 Ni(II) formulation, in keeping with the metallaepoxide extreme of the Dewar-Chatt-Duncanson (DCD) model of bonding (Scheme 1). In addition, preliminary density functional theory (DFT) calculations (*vide infra*) revealed *prohibitively* high barriers to rotation of the π-ligand (*i.e.* 80-100 kJ/mol), demonstrating that these complexes are indeed square planar and not trigonal with a freely rotating π-ligand. We have previously reported similar high barriers to rotation with a rhodium-olefin system.[8] Indeed, the metallaepoxide electromer of related nickel complexes have recently been invoked by the groups of Doyle[41] and Ogoshi[36] based on reactivity studies, and is also shown explicitly in Group 4 complexes that display similar structural parameters to the nickel species discussed here.[57–62]

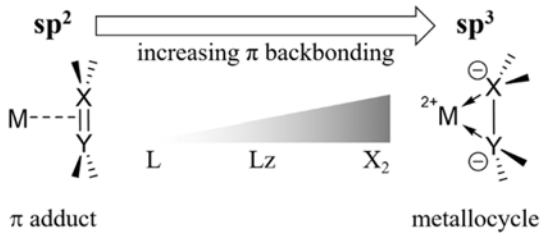

Scheme 1 Continuum of possible electronic configurations for binding of a π-system to a redox-active metal centre. On the left, is the limiting case of simple π adduct formation, where M-L binding occurs via σ donation from the π system. As π-backbonding increases, the X=Y π bond weakens and, in the limit, a metallacycle is formed with loss of the π bond and formal $2e^-$ oxidation at the metal centre.

The ambiguity in the electronic structure description of these nickel π complexes is as yet unresolved, which hinders efforts towards rational design of nickel-catalysed processes. We thus set out to investigate the bonding and electronic structure of a family of nickel dtbpe complexes by utilizing a combination of spectroscopic and computational techniques. This study is also relevant to the ongoing discussion about the value of formal oxidation states.[63–65] Overall, we have found that these systems are dominated by π-backbonding with minimal *σ*-donation from the ligand; the degree of backbonding reflects the energy difference between the filled nickel 3*d* orbitals and the π* orbitals on the ligand as well as important contributions from the diphosphine ligand. We believe that this insight will prove beneficial to both the logical improvement of known catalytic reactions with nickel and to the rational design of new transformations. We describe herein the details of this study.

Results

Solid-state molecular structures

We selected a variety of (dtbpe)Ni complexes ranging from well-defined nickel(II) complexes to π-complexes of organic molecules (Charts 1-3). The complexes split into two categories based on the dihedral angles observed in the solid-state structures: (i) those with near planar geometries (**1-12**, where $\varphi_{dih} \sim 0°$ and $\sum\measuredangle_{Ni} \sim 360°$) and those with pseudo-tetrahedral geometries at the nickel centre (**13-15**, where $\varphi_{dih} \sim 90°$ and $\sum\measuredangle_{Ni} \sim 440°$). Alternatively, differences in the geometry of four-coordinate complexes can be evaluated using τ_4 values, which range from $\tau_4^{(D_{4h})} = 0$ to $\tau_4^{(T_d)} = 1$.[66] This approach confirms the *pseudo*-tetrahedral ($\sim T_d$) geometry of **13-15** (Chart 3) but suggests that the more planar complexes split into a set of highly symmetrical square planar complexes (Chart 2) and a set of complexes that deviate more strongly from idealized D_{4h} symmetry (Chart 1). The latter complexes are all π-complexes where the deviation from an idealized geometry results from the extremely small bite angle formed by the π ligand (when considered as an η^2 ligand), even while maintaining planarity. The planar geometry at the metal centre implies that **1-7** must exhibit large degrees of backbonding,

leading to formally square planar Ni(II) d^8 complexes (*i.e.*, a metallocyclic electronic configuration as depicted in Scheme 1).

		τ_4	$\Sigma\measuredangle_{Ni}$	$J_{P,P}$ (Hz)
8	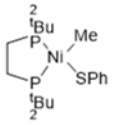	0.08	360.9°	4
9	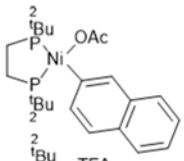	0.11	360.6°	-
10	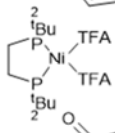	0.04	360.1°	-
11	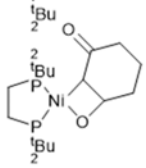	0.13	359.8°	6
12	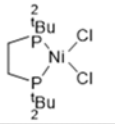	0.11	361.1°	-
	average	0.09	360.5°	5

Chart 2. List of reference Ni(II) square planar complexes, which exhibit both small $^2J_{PP}$ coupling constants (where available) and τ_4 values.

The structure of the π ligand itself has also often been used to estimate the degree of backbonding; electron donation into the ligand π* orbital *via* backbonding should lead to bond elongation. For example, Zeise's salt [$KPtCl_3(C_2H_4)$] and Cramer's dimer [$Rh(C_2H_4)_2Cl]_2$, both commonly used organometallic starting materials, feature short C=C ethylene bond distances of 137.5 pm[67] and 139.5 pm[68], respectively. In contrast, (MeTPA)Rh(C_2H_4)(BPh_4), features a much longer C=C bond distance of 145 pm,[69] which corresponds to the metallacyclopropane end of the DCD spectrum. However, this method is generally qualitative, with many examples that fall in the middle of the spectrum being simply described as hybrids of the two resonance forms.[70,71] Indeed, the C=O bond lengths of the η²-carbonyl complexes examined here (complexes **1**, **2**, **3** and **6**) all fall between 131.7-135.4 pm. This range is unfortunately ambiguous, as it is in the middle of the typical bond lengths of ~122 pm and ~143 pm for C=O double bonds and C-O single bonds, respectively. Similarly, information about the degree of backbonding can be gleaned from the sum of the bond angles about the carbon atom of the π-unit ($\sum\measuredangle_C$, Chart 1). However, these results are again inconclusive, as the observed $\sum\measuredangle_C\,(=341-352°)$ are intermediate between those expected for planar sp^2-hybridized and pyramidalized sp^3-hybridized carbon atoms. This approach also suffers from the fact that many π-ligands bear hydrogen substituents, which can be difficult to locate using traditional XRD[72] and occasionally require neutron diffraction experiments to accurately ascertain their positions.

		τ_4	$\Sigma\measuredangle_{Ni}$
13	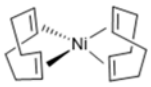	0.89	411.4°
14	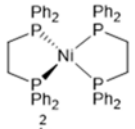	0.81	424.8°
15	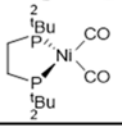	0.93	429.7°
	average	0.88	422.0°

Chart 3. List of reference pseudo-tetrahedral Ni(0) complexes, with large τ_4 values and $\sum\measuredangle_{Ni} > 400°$.

Nuclear magnetic resonance spectroscopy

A common approach for evaluating the oxidation state of metals in diphosphine complexes involves using the magnitude of P,P-scalar coupling constants ($^2J_{P,P}$). In nickel chemistry, it is generally observed that small $^2J_{P,P}$ (i.e. 2-30 Hz) correspond to nickel(II) complexes whereas larger $^2J_{P,P}$ (i.e. 45-80 Hz) correspond to nickel(0) complexes.[10,11,80,21,73–79] However, exceptions to this trend have been reported by ourselves[10] and others.[79,81] Moreover, this approach is necessarily limited to asymmetric species given that $^2J_{P,P}$ cannot be observed in complexes such as **4** and **7** due to symmetry. To the best of our knowledge, a study relating the magnitude of these coupling constants and how they correlate with alternate spectroscopic approaches has not been performed. We turned to X-ray absorption spectroscopy (XAS) and X-ray emission spectroscopy (XES) for an independent evaluation of the electronic structure and spectroscopic oxidation states.

Ni K-edge X-ray absorption spectroscopy

In principle, the spectroscopic oxidation state of the metal ion can be quite accurately assigned *via* the energy of either the ionization edge and/or the energy of low-energy pre-edge features in the metal K-edge near-edge spectrum.[82–88] Ni K-edge XAS can therefore be used to explore the spectroscopic oxidation state of a wide range of nickel-containing species.[89–93]

We obtained high-quality Ni K-edge XAS data on several Ni π-complexes in addition to several reference complexes from Chart 1. Near-edge spectra for 'classic' Ni(II) complexes such as that for complex **12** have well-resolved pre-edge features: a weak feature at ~8333 eV and a more intense feature at ~8336 eV.

The more intense feature in such complexes has previously been ascribed to a dipole-allowed Ni 1s → 4p contribution whereas the weaker feature results from the electric-quadrupole allowed Ni 1s → 3d transition.[94,95] By contrast, Ni π-complexes (such as **1**, **2**, **4**, and **7**) have a markedly different

edge profile and only one clearly resolvable intense pre-edge feature that ranges from 8333-8336 eV depending on the complex. Similar spectroscopic behaviour has previously been observed in copper(I)-derived π complexes.[83] As for the copper systems, the energy of the Ni 1s → 4p feature in the rising edge appears to correlate with the oxidation state of the metal centre. The weaker pre-edge feature is not directly resolvable in most complexes although in complexes **1** & **2**, a weak low-energy shoulder is observed in the 2nd derivative of the spectra (see SI 04).

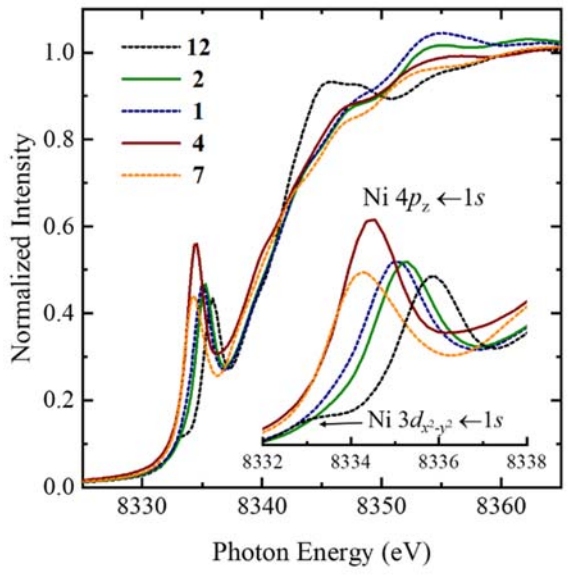

Figure 1. Normalized Ni K-edge PFY XANES edge spectra for Ni(dtpe)Cl_2 (**12**), Ni(dtbpe)(benzene) (**7**), Ni(dtbpe)(ethylene) (**4**), Ni(dtbpe)CF_3COOEt (**1**), and Ni(dtbpe)CF_3COOEt (**2**). The pre-edge region for each of the spectra is shown in the inset with assignments for the observed features.

Ni Kβ X-ray emission spectroscopy

To further probe the charge distribution in these complexes, we obtained Ni Kβ emission data for some of the complexes. The intensity-weighted average energy of the Kβ line for each of the complexes suggests that all of the Ni π-complexes have a similar Z_{eff} (see SI 35). The trend is similar to that obtained from the energies of the Ni 1s → 4p feature in the Ni K-edge XAS but the emission energies for the π-complexes are quite similar (< 1 eV) and well separated from the observed energy of **12**. The similarity in the Kβ emission data for all of the π complexes seems to support a common formal oxidation state for **1**-**7**.

Computational Studies - Density Functional Theory

DFT calculations were performed on each of the species in Chart 1, using simplified diphosphine ligands (See SI 01 for details). Molecular structures derived from B3LYP/def2-TZVP calculations of the dtbpe complexes, as well as those using a simplified diphosphine ligand (dmpe = 1,2-bis(dimethylphosphino) ethane)[a] yield good agreement with solid-state molecular structures of **1**-**12**.[10,11,21,56,96,97] The effect of decreasing the steric bulk and electron donation in the supporting diphosphine ligand does not affect the general structural trends and conclusions, which are consistent with those observed in the experimental data. Furthermore, the spectroscopic features observed in the Ni K-edge XAS data are well reproduced using TD-DFT analysis. Although qualitative results were consistent across a broad range of functionals, results from B3LYP provided the best agreement with experimental pre-edge features. Basis set effects were observed to be minimal beyond TZVP. The strong agreement with experimental data suggests that our DFT results should provide a reasonable description of bonding in these species.

The Ni K-edge pre-edge features are extremely sensitive to electron distribution (Figure 2). The more intense higher energy ($Ni\ 4p \leftarrow 1s$) transition increases with greater oxidation at the metal centre and reproduces the trend observed in the experimental data. The weaker low energy transition ($Ni\ 3d \leftarrow 1s$) shifts in the opposite direction, such that the energy difference between the two features (ΔE_{dp}) increases with increasing oxidation at the metal centre. The weak low-energy 3d feature should eventually be unresolvable from the higher intensity 4p feature, as observed in the experimental data.

The nature of the two pre-edge final states is consistent across the series of π-complexes. The intense feature results from a transition to the *non-bonding* Ni $4p_z$ orbital, whose energy directly reflects the effective nuclear charge at the metal centre. The weaker feature corresponds to a transition to the formally *ligand-based antibonding* π* orbital, which gains electric quadrupole character through mixing with the Ni $3d_{x^2-y^2}$ orbital through π backbonding. In principle, the intensity of this features should therefore reflect the degree of M-L π backbonding. However, the intensity of this pre-edge feature also depends on the degree of Ni d-p mixing, which varies across the series. This contribution, in addition to the difficulty of resolving weak pre-edge shoulder, makes it challenging to directly quantify the degree of backbonding from the experimental data.

To further explore the electron distribution in the ground state of these π systems, we applied charge decomposition (CDA),[98,99] natural bond orbital (NBO),[100] and atoms-in-molecules (QTAIM)[101] analyses to these Ni π systems. Together, these provide a comprehensive view of the electronic properties of these systems. In all cases, the predominant interactions between the metal ion and the π ligand can be well described using the basic interactions defined within the DCD bonding model.

[a] Computed structures using the dmpe ligand are labeled using a ' (prime) in the numbering. For example, **4'** is simply complex **4** from Chart 1 that has been calculated using the simplified dmpe ligand rather than the full dtbpe ligand.

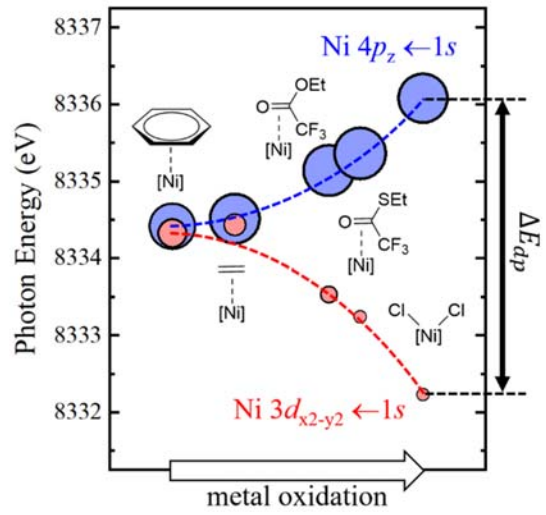

Figure 2. Calculated Ni K-edge XANES TD-DFT results for pre-edge region of the spectrum. Each complex is represented by a blue circle (Ni $4p_z \leftarrow 1s$) and a red circle (Ni $3d_{z2-y2} \leftarrow 1s$). The area of the of each circle is proportional to the calculated oscillator strength (f_{osc}) for each transition. All calculated TD-DFT energies at the Ni K-edge were shifted by -98.55 eV. A more complete set of TD-DFT results are presented in Figure SXX.

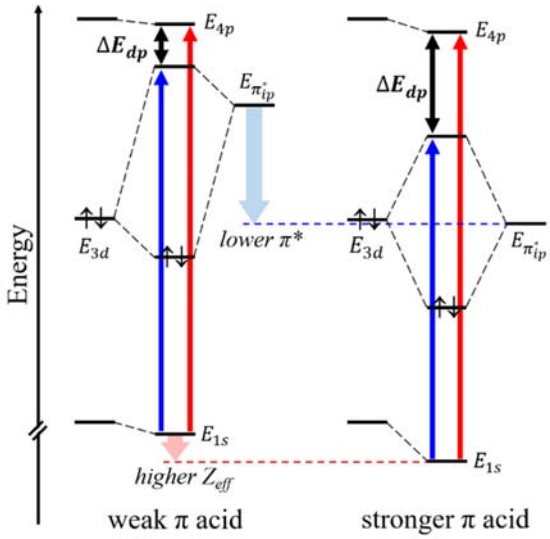

Figure 3. Simplified MO diagram depicting differences between weaker (left, *e.g.* ethylene in **4**) and stronger π acidic ligands (right, e.g. cyclohexanone in **6**). Greater π acidity leads to a much lower π^*_{ip} and thus greater π backbonding. Decreased electron density at the metal centre (i.e. increased Z_{eff}) also lowers the energy of the Ni 1s orbital. These two effects lead to a simultaneous increase in energy of the Ni 1s → 4p transition (red arrow) and decrease in energy of the Ni 1s→ π* (blue arrow) and therefore an increase in the splitting of the two acceptor orbitals (ΔE_{dp}). Quantitative results are given in supporting information as SI 41.

Most notably, π backbonding is the dominant contribution to bonding in these systems. The electron rich metal centre does not accept significant electron density through σ donation from the π_b ligand orbital with only minimal charge donation into the higher lying empty Ni 4s/p orbitals. The π backbonding interaction involves overlap between the Ni $3d_{x2-y2}$ and the in-plane ligand π^* (π^*_{ip}). As expected, the overall degree of charge transfer correlates directly with the relative energies of these contributing fragment orbitals (see SI 41). Given that the Ni(dtbpe) fragment is identical in all cases, differences within the series result primarily from changes in the energy of the ligand π^*_{ip} orbital. As summarized in Figure 3, poorer π acids such as olefins have a higher energy $E_{\pi^*_{ip}}$ and thus should exhibit a small ΔE_{dp}, whereas $E_{\pi^*_{ip}}$ is lower in energy for stronger π acids (such as carbonyls), increasing backbonding and a larger ΔE_{dp}.This interaction leads to a surprisingly large barrier for ligand rotation, even for those where backbonding is least important: barriers of ~100 kJ/mol are obtained for both symmetric (**4**) and asymmetric (**3**) π ligands.

Although the above analysis is valid for all species investigated, there is one additional factor that contributes to the nature of the bonding in these systems. The significant electronegativity difference between carbon and oxygen in the carbonyl π ligands leads to asymmetry in the orbitals involved in bonding. The nature of bonding in these asymmetric systems is therefore more complex and deviates somewhat from the simple DCD model as σ donation becomes more localized from the terminal oxygen atom and π backbonding localizes onto the electron deficient carbonyl carbon atom. This localization is also consistent with π backbonding (to C) being stronger than σ donation (from O), as observed from bond strength parameters in Table 1.

Table 1. Wiberg bond indices for Ni-C, Ni-X (X=O or most electron-rich C), and QTAIM $\nabla^2(\rho_{DFT})$ for optimized complexes at B3LYP/def2-TZVP level of theory.

		Wiberg Indices		$\nabla^2(\rho_{DFT})$		
		Ni-C	Ni-X	bcp_{NiC}	bcp_{NiX}	rcp_{NiCO}
C=C	**7'**	0.362	0.357	0.217	0.224	0.309
	5'	0.495	0.403	0.213	0.261	0.353
	4'	0.486	0.487	0.235	0.238	0.359
C=O	**3'**	0.516	0.487	0.524	0.248	-
	1'	0.556	0.468	0.550	0.219	-
	2'	0.552	0.502	0.537	0.243	-
	6'	0.523	0.494	0.536	0.232	-

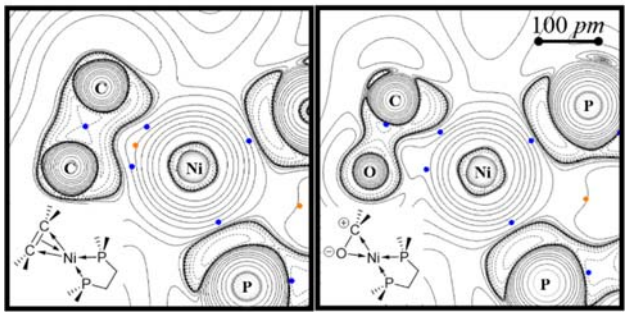

Figure 4. QTAIM topological analysis for complexes **4'** (left) and **1'** (right). Contour maps of $\nabla^2(\rho_{DFT})$ in the NiCX plane (X=C, O). Dotted contours refer to positive values of $\nabla^2(\rho_{DFT})$ and solid lines to negative values of $\nabla^2(\rho_{DFT})$. Bond critical points are shown in blue and ring critical points are shown in red. A simplified representation of these bonding interactions is shown on the bottom left of for each of the complexes.

The effect of π ligand asymmetry is also clearly observed in the QTAIM analysis: Figure 4 shows a comparison of the Laplacian of the DFT-derived electron density ($\nabla^2(\rho_{DFT})$) for **4'** and **1'**. In the olefinic π-complex, the electron density within the Ni-C-C

trigonal core reveals two Ni-C bond critical points (bcp) and one ring critical point (rcp) that connects all three atoms. The rcp correlates with a σ donor interaction due to π_{CC} donation in the Ni $3d_{xy}$ orbital and the two Ni-C bcp's correspond to π-backbonding from the Ni $3d_{x^2-y^2}$ and the ligand π^*_{ip}. By contrast, $\nabla^2(\rho_{DFT})$ for **1'** is highly asymmetric with two bcp's (Ni-O and Ni-C) but no discernible rcp in this case.

Discussion

Our studies of a series of nickel π-complexes reveal interesting electronic structure features that can be rationalized within the context of the DCD bonding model. The spectroscopic characteristics of these species are highly sensitive to the nature of bonding to the π ligand, more specifically the properties of the species are intimately linked to the degree of π backbonding from the electron rich metal centre. Taken together, our studies allow for a more concrete evaluation of the factors that control this bonding and their implications.

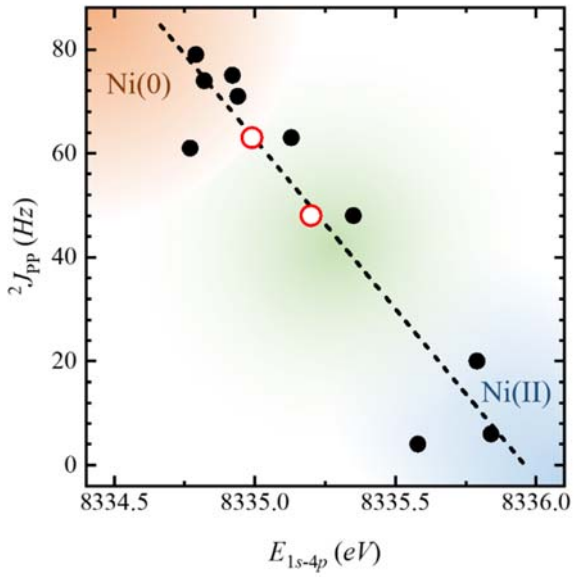

Figure 5. Correlation between Ni 1s→4p transition energies and $^2J_{PP}$ NMR coupling constants. Data points in black circles are from TDDFT calculations whereas those in red circles are from experimental Ni K-edge XAS data. All TD-DFT calculated transition energies were linearly shifted by -98.55 eV. The dashed line represents a linear correlation fit ($R^2 = 0.87$); see SI 3.

Oxidation states of nickel diphosphines are often evaluated *via* the magnitude of $^2J_{P,P}$ in unsymmetrical complexes: a small coupling constant ($2Hz < {}^2J_{P,P} < 30Hz$) correlates with Ni(II) complexes, whereas large coupling constants ($45Hz < {}^2J_{P,P} < 80Hz$) are associated with Ni(0) species. Differences reflect the electron density at the metal centre, which bridges the two ^{31}P atoms.[102] There is little evidence regarding potential Ni(I) species given the challenges associated with obtaining such information in paramagnetic species.[13,76] XAS offers the advantage of providing an independent experimental probe requiring neither inequivalent phosphorus ligands nor diamagnetism. As noted previously, the XAS data of formally square planar complexes yield distinctive pre-edge features that track with oxidation of the metal centre. The NMR coupling constants and XAS pre-edge energies correlate extremely well (Figure 5), providing good support that $^2J_{P,P}$ (where available) are useful in defining electron density at the metal centre.

The fact that the two pre-edge features in the Ni K-edge XAS data respond so differently to changes in the electronic structure implies that they are sensitive to different aspects of the electronic structure of the metal centre. The Ni $4p_z$ orbital is out-of-plane from the most important ligand field interactions in pseudo square planar geometries and thus reports directly on Z_{eff} of the metal centre. In contrast, the weak pre-edge feature is a predominantly in-plane ligand-based final state with some metal $3d_{x^2-y^2}$ character. The two features therefore behave very differently with the former reporting on Z_{eff} of the metal centre and the latter on differences in the ligand field.

The DCD model is a simple yet powerful approach for explaining the behaviour of π-complexes in transition metal chemistry. Its limitations have recently been explored in copper dioxygen and related systems by invoking the important contributions of static correlation, specifically by allowing for multi-determinant solutions.[83] Since the electron density of these systems are well described from DFT calculations, we approached this same issue by applying natural resonance theory[103–105] (NRT) to expose different contributions to the overall electronic description.[8] In all cases, the Ni(II) metallacycle contributes little to the overall electronic structure. The Ni(0) π adduct and Ni(I) intermediate resonance structures account for >80% of the electronic structure in all cases. Indeed, we find that the Ni(0) π adduct is the largest contributor for all the structures examined, although Ni(I) contributions are non-negligible.

Table 1. Summary of NRT analyses for complexes with either olefin or carbonyl π ligands.

		Ni(0)	Ni(I)	Ni(II)
C=C	**7'**	67%	33%	0%
	5'	56%	37%	7%
	4'	51%	36%	10%
C=O	**3'**	57%	38%	5%
	1'	48%	47%	4%
	2'	46%	43%	11%

The high barrier to rotation for π ligands in these complexes implies a surprisingly strong preference for a planar geometry even though a closed-shell Ni(0) π adduct should not behave in this way. Even more surprisingly, the barrier to rotation does *not* correlate strongly with the degree of Ni(I) character from our NRT analysis. This effect points to the importance of the trans diphosphine ligand in enabling and supporting π backbonding. In principle, π backbonding in a d^{10} Ni(0) occurs in any geometry of the π ligand because of availability of filled Ni $3d_{xz,yz}$ orbitals that could also support backbonding. However, the C=C bond distance (r_{CC}) decreases significantly upon ligand rotation (from 147 to 139 pm), indicating that backbonding is not well supported in alternate geometries. The electronic

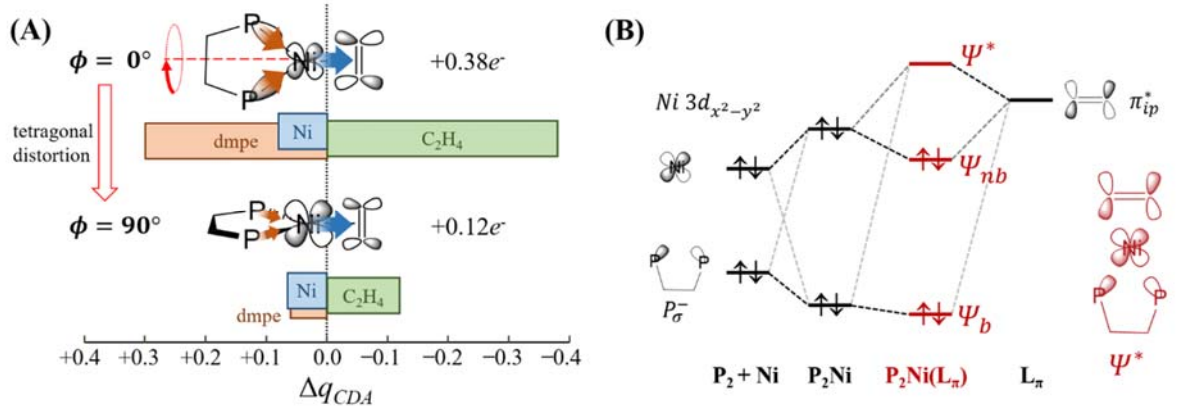

Figure 6. (**A**) DFT-calculated charge donation from CDA analysis for ethylene complex with dmpe ligand (**4'**) for ground state geometry ($\phi = 0°$) and after tetragonal distortion (rotation of NiCC plane relative to NiPP plane, $\phi = 90°$). Backbonding decreases substantially due to large drop in phosphine σ donation into the Ni $3d_{x2\text{-}y2}$. (**B**) Qualitative molecular orbital representation of the 3c4e bonding that connects P_σ^- with π_{ip}^* via the Ni $3d_{x^2-y^2}$ orbital.

changes that occur upon rotation of the π ligand are an indicator of the importance of the diphosphine ligand.

Charge donation from the P_2Ni fragment to the π ligand decreases substantially when the diphosphine ligand is perpendicular to the Ni $3d_{x^2-y^2}$ donor orbital (Figure 6A). This suggests that the metal centre in these complexes mediates charge donation from the electron rich diphosphine to the ethylene π*. The orbital contributions that allow for π backbonding are reminiscent of a classical 3c-4e bond; in this situation the three contributing orbitals are the antisymmetric combination of the phosphine σ-donor orbitals (P_σ^-, 2 valence electrons), the Ni $3d_{x^2-y^2}$ (2 valence electrons), and the ligand π_{ip}^* orbital (Figure 6B). In this geometry, the two sets of ligands generate a cooperative "push-pull" system mediated by the metal centre in a manner similar to that which has been observed in cytochrome P450s.[106]

Although all of the olefin complexes investigated are best described as Ni(0) complexes, highly electron poor carbonyl complexes are significantly more oxidized. Complexes **1** and **2** represent intriguing examples of intermediate cases that are shifting towards a "Ni(I)"-type description. The CF_3 substituent at the carbonyl carbon increases their π acidity substantially. However, the ester ligand in **1** is less π acidic than the equivalent thioester in **2** due to better delocalization of the ligand π system, which simultaneously decreases overlap of the π* with the Ni $3d_{x2\text{-}y2}$ and increases its energy. In **2**, poor π overlap between the larger atomic orbitals on sulphur and the carbonyl π* allows for significant backbonding in this case. These differences should lead to concomitant differences in reactivity. Indeed, **1** and **2** display fundamentally different reactivity. In refluxing benzene, **2** slowly thermolyzes over two days, resulting in complex **15**, free ligand, and thioester, as determined by ^{31}P and ^{1}H NMR spectroscopy. In contrast, complex **1** is stable for up to a week under the same conditions with no sign of decomposition. Complex **1** does not react with MeLi, even upon prolonged reflux in benzene, but under the same conditions, complex **2** reacts with MeLi to form trace amounts of EtSSEt. In addition, complex **2** is susceptible to cross-coupling with phenylboronic acid, forming PhSEt in moderate (35%) yield.[11] No such cross-coupling reactivity was observed with complex **1**. Lastly, complexes **1** and **2** react differently with MeI. Upon refluxing in benzene for 12 hours, **1** forms (dtbpe)Ni(Me)(I),[107] which was verified by ^{31}P NMR spectroscopy, and liberates the free ester, whereas complex **2** does not react with MeI at all under the same conditions.[a] Such behaviour is consistent with reduced π donation of the ester in **1**, allowing for its displacement by MeI.

Conclusions

Our spectroscopic and computational studies on a series of Ni π-complexes shed light on a seemingly paradoxical electronic and geometric structure: the existence of stable square-planar d^{10} complexes. In the case of olefinic complexes, the evidence shows that these are best described as Ni(0) π adducts with strong π-backbonding coupled to in-plane σ donation from the supporting electron rich diphosphine bidentate ligand. The formation of this 3c-4e interaction generates ligand σ-to-π (Lσ→Lπ) charge transfer. This push-pull ligand effect is responsible for the large observed rotational barrier about the π ligand even with relatively poor π acidic ligands such as ethylene. This unique electronic structure can play an important role in the reactivity of such species.[108] The situation is more complex in situations with highly electron poor π systems, where metal-centred backbonding increases and keads to Ni(I) character becomes significantly more important. There are clear implications for reactivity of these common organometallic intermediates and we anticipate that more detailed studies of ancillary ligand effects in such systems are warranted.

Conflicts of interest

There are no conflicts to declare.

Acknowledgements

This work was supported by the Natural Sciences and Engineering Research Council of Canada (NSERC) via Discovery grants and Research Tools and Instrumentation grants to J.A.L. and P.K. Scholarship support was provided to A.N.D. by NSERC (CGS-D3 + MSFSS), the University of British Columbia (Laird + 4YF), and the Izaak Walton Killam Foundation during his graduate studies. W.H. is grateful for support in the form of a MITACS Globalink doctoral fellowship. W.C. is grateful for support from the NSERC CREATE SusSyn program.
This work is partially based upon research performed at the Stanford Synchrotron Radiation Lightsource (SSRL) at the SLAC National Accelerator Laboratory. Use of SSRL is supported by the U.S. Department of Energy, Office of Science, Office of Basic Energy Sciences under Contract No. DE-AC02-76SF00515. This work is partially based upon research conducted at the Cornell High Energy Synchrotron Source (CHESS) which is supported by the National Science Foundation under award DMR-1332208. This research was enabled in part by support provided by WestGrid (www.westgrid.ca) and Compute Canada Calcul Canada (www.computecanada.ca).

Experimental

General Considerations

Unless stated otherwise, all reactions were performed in a glovebox or on a Schlenk line under an atmosphere of pure N_2 using standard Schlenk techniques. Anhydrous pentanes, toluene, diethyl ether, and tetrahydrofuran were purchased from Aldrich, sparged with N_2, and dried further by passage through towers containing activated alumina and molecular sieves. C_6H_6 and C_6D_6 were purchased from Aldrich and dried over sodium/benzophenone before being distilled and degassed by three freeze-pump-thaw cycles. CD_2Cl_2 was purchased from Aldrich and dried over CaH_2 before being distilled and degassed by three freeze-pump-thaw cycles. $Ni(COD)_2$ (**13**) was purchased from Strem and used as received. Complexes **1-12** and **14-15** were prepared and purified according to literature procedures.[10,11,56,96,107,109,110] All other chemicals were purchased from commercial suppliers and used as received.

X-ray Absorption Spectroscopy

All the XAS samples were analyzed as solids under anaerobic conditions and diluted in boron nitride (20-50% by weight). XAS Ni K-edges were acquired at the SSRL beamline 7-3, which is equipped with a Si(220) φ = 90° double crystal monochromator, a 9 keV cutoff mirror, and a He cryostat (at 20 K). Data were collected using a Canberra 30-element Ge solid-state detector with a 3mm Co filter. Data averaging and energy calibration were performed using SixPack[111] and the AUTOBK algorithm available in the Athena software package[112] was employed for data reduction and normalization.

X-ray emission spectroscopy

Samples were prepared for XES by pressing finely ground powders into 1 mm Al spacers, and sealing with 40 µm Kapton tape. Data were obtained at the Cornell High Energy Synchrotron Radiation Source (CHESS) at the C-line end station. Energy selection was performed with upstream multilayers, providing ~50 eV band pass. A Rh-coated harmonic rejection mirror was also utilized. Kβ X-ray emission spectra were measured using a spherical analyzer (using the 620 reflection of three Ge 310 analyzer crystals) in combination with a silicon drift detector aligned in Rowland geometry. Data were normalized with respect to the incident flux in an upstream N_2-filled ionization chamber. Data were collected at ~20 K in a Displex cryostat to minimize photoreduction.

Computational methods

Initial geometries for all molecules were obtained from crystallographic coordinates (where available) or constructed from standard models. Geometry optimizations and numerical frequency calculations were performed using version 3.0.3 of the ORCA computational chemistry package. Molecular geometries were optimized using the B3LYP functional in combination with the Ahlrichs triple-ζ basis set with valence polarization (def2-TZVP) for all atoms. Computational efficiency was improved by applying the RI approximation (RIJCOSX) for the hybrid functional. All calculations were performed with integration grid 4. Reported thermochemical energies are given in kJ/mol and correspond to Gibbs free energies (ΔG^0) with zero-point vibrational energy corrections (ZPVE). NBO results were obtained using Gaussian 09; AIM and CDA calculation were performed in Multiwfn software from NBO outputs. All calculations were run on either the Abacus (UBC Chemistry) or GREX (Westgrid) computing clusters.

Notes and references

a Both **1** and **2** react with HCl to make (dtbpe)NiCl2 (**12**) and PhLi to form moderate but irreproducible amounts of biphenyl.

1 O. R. Luca and R. H. Crabtree, *Chem. Soc. Rev.*, 2013, **42**, 1440–1459.
2 V. Lyaskovskyy and B. de Bruin, *ACS Catal.*, 2012, **2**, 270–279.
3 P. J. Chirik and K. Wieghardt, *Science (80-.).*, 2010, **327**, 794–795.
4 M. W. Bouwkamp, A. C. Bowman, E. Lobkovsky and P. J. Chirik, *J. Am. Chem. Soc.*, 2006, **128**, 13340–13341.
5 H. Nishiyama, H. Ikeda, T. Saito, B. Kriegel, H. Tsurugi, J. Arnold and K. Mashima, *J. Am. Chem. Soc.*, 2017, **139**, 6494–6505.
6 K. J. Blackmore, J. W. Ziller and A. F. Heyduk, *Inorg. Chem.*, 2005, **44**, 5559–5561.
7 B. de Bruin, M. J. Boerakker, J. J. J. M. Donners, B. E. C. Christiaans, P. P. J. Schlebos, R. de Gelder, J. M. M. Smits, A. L. Spek and A. W. Gal, *Angew. Chemie Int. Ed. English*, 1997, **36**, 2064–2067.
8 A. N. Desnoyer, S. Behyan, B. O. Patrick, A. Dauth, J. A. Love and P. Kennepohl, *Inorg. Chem.*, 2016, **55**, 13–15.
9 P. H. M. Budzelaar and A. N. J. Blok, *Eur. J. Inorg. Chem.*, 2004, **2004**, 2385–2391.
10 A. N. Desnoyer, E. G. Bowes, B. O. Patrick and J. A. Love, *J. Am. Chem. Soc.*, 2015, **137**, 12748–12751.

11 A. N. Desnoyer, F. W. Friese, W. Chiu, M. W. Drover, B. O. Patrick and J. A. Love, *Chem. - A Eur. J.*, 2016, **22**, 4070–4077.

12 N. A. LaBerge and J. A. Love, *European J. Org. Chem.*, 2015, **2015**, 5546–5553.

13 D. D. Beattie, E. G. Bowes, M. W. Drover, J. A. Love and L. L. Schafer, *Angew. Chemie Int. Ed.*, 2016, **55**, 13290–13295.

14 D. R. Hartline, M. Zeller and C. Uyeda, *J. Am. Chem. Soc.*, 2017, **139**, 13672–13675.

15 D. J. Mindiola, *Angew. Chemie Int. Ed.*, 2009, **48**, 6198–6200.

16 P. Zimmermann and C. Limberg, *J. Am. Chem. Soc.*, 2017, **139**, 4233–4242.

17 E. B. Corcoran, M. T. Pirnot, S. Lin, S. D. Dreher, D. A. DiRocco, I. W. Davies, S. L. Buchwald and D. W. C. MacMillan, *Science (80-.).*, 2016, **353**, 279–283.

18 B. A. Vara, X. Li, S. Berritt, C. R. Walters, E. J. Petersson and G. A. Molander, *Chem. Sci.*, 2018, **9**, 336–344.

19 B. P. Woods, M. Orlandi, C.-Y. Huang, M. S. Sigman and A. G. Doyle, *J. Am. Chem. Soc.*, 2017, **139**, 5688–5691.

20 C. Heinz, J. P. Lutz, E. M. Simmons, M. M. Miller, W. R. Ewing and A. G. Doyle, *J. Am. Chem. Soc.*, 2018, **140**, 2292–2300.

21 M. L. Lejkowski, R. Lindner, T. Kageyama, G. É. Bódizs, P. N. Plessow, I. B. Müller, A. Schäfer, F. Rominger, P. Hofmann, C. Futter, S. A. Schunk and M. Limbach, *Chem. - A Eur. J.*, 2012, **18**, 14017–14025.

22 M. Al-Ghamdi, S. V. C. Vummaleti, L. Falivene, F. A. Pasha, D. J. Beetstra and L. Cavallo, *Organometallics*, 2017, **36**, 1107–1112.

23 Z. R. Greenburg, D. Jin, P. G. Williard and W. H. Bernskoetter, *Dalt. Trans.*, 2014, **43**, 15990–15996.

24 I. Knopf, D. Tofan, D. Beetstra, A. Al-Nezari, K. Al-Bahily and C. C. Cummins, *Chem. Sci.*, 2017, **8**, 1463–1468.

25 C. Hendriksen, E. A. Pidko, G. Yang, B. Schäffner and D. Vogt, *Chem. - A Eur. J.*, 2014, **20**, 12037–12040.

26 N. Huguet, I. Jevtovikj, A. Gordillo, M. L. Lejkowski, R. Lindner, M. Bru, A. Y. Khalimon, F. Rominger, S. A. Schunk, P. Hofmann and M. Limbach, *Chem. - A Eur. J.*, 2014, **20**, 16858–16862.

27 D. Jin, P. G. Williard, N. Hazari and W. H. Bernskoetter, *Chem. - A Eur. J.*, 2014, **20**, 3205–3211.

28 S. Manzini, N. Huguet, O. Trapp and T. Schaub, *European J. Org. Chem.*, 2015, **2015**, 7122–7130.

29 W. Guo, C. Michel, R. Schwiedernoch, R. Wischert, X. Xu and P. Sautet, *Organometallics*, 2014, **33**, 6369–6380.

30 N. Saito, Z. Sun and Y. Sato, *Chem. - An Asian J.*, 2015, **10**, 1170–1176.

31 S. C. E. Stieber, N. Huguet, T. Kageyama, I. Jevtovikj, P. Ariyananda, A. Gordillo, S. A. Schunk, F. Rominger, P. Hofmann and M. Limbach, *Chem. Commun.*, 2015, **51**, 10907–10909.

32 S. Ogoshi, Y. Hoshimoto and M. Ohashi, *Chem. Commun.*, 2010, **46**, 3354.

33 Y. Hoshimoto, M. Ohashi and S. Ogoshi, *J. Am. Chem. Soc.*, 2011, **133**, 4668–4671.

34 Y. Hoshimoto, M. Ohashi and S. Ogoshi, *Acc. Chem. Res.*, 2015, **48**, 1746–1755.

35 R. Kumar, Y. Hoshimoto, H. Yabuki, M. Ohashi and S. Ogoshi, *J. Am. Chem. Soc.*, 2015, **137**, 11838–11845.

36 Y. Hoshimoto, H. Yabuki, R. Kumar, H. Suzuki, M. Ohashi and S. Ogoshi, *J. Am. Chem. Soc.*, 2014, **136**, 16752–16755.

37 Y. Bernhard, B. Thomson, V. Ferey and M. Sauthier, *Angew. Chemie Int. Ed.*, 2017, **56**, 7460–7464.

38 Y. Kita, R. D. Kavthe, H. Oda and K. Mashima, *Angew. Chemie Int. Ed.*, 2016, **55**, 1098–1101.

39 Y. Kita, H. Sakaguchi, Y. Hoshimoto, D. Nakauchi, Y. Nakahara, J.-F. Carpentier, S. Ogoshi and K. Mashima, *Chem. - A Eur. J.*, 2015, **21**, 14571–14578.

40 M. S. Azizi, Y. Edder, A. Karim and M. Sauthier, *European J. Org. Chem.*, 2016, **2016**, 3796–3803.

41 D. K. Nielsen and A. G. Doyle, *Angew. Chemie Int. Ed.*, 2011, **50**, 6056–6059.

42 K. Muto, J. Yamaguchi, D. G. Musaev and K. Itami, *Nat. Commun.*, 2015, **6**, 7508.

43 M. L. Smith, A. K. Leone, P. M. Zimmerman and A. J. McNeil, *ACS Macro Lett.*, 2016, **5**, 1411–1415.

44 A. K. Leone and A. J. McNeil, *Acc. Chem. Res.*, 2016, **49**, 2822–2831.

45 P. Willot and G. Koeckelberghs, *Macromolecules*, 2014, **47**, 8548–8555.

46 S. R. Lee, J. W. G. Bloom, S. E. Wheeler and A. J. McNeil, *Dalt. Trans.*, 2013, **42**, 4218.

47 Z. J. Bryan and A. J. McNeil, *Chem. Sci.*, 2013, **4**, 1620.

48 S. R. Lee, Z. J. Bryan, A. M. Wagner and A. J. McNeil, *Chem. Sci.*, 2012, **3**, 1562.

49 E. L. Lanni, J. R. Locke, C. M. Gleave and A. J. McNeil, *Macromolecules*, 2011, **44**, 5136–5145.

50 H. Komber, V. Senkovskyy, R. Tkachov, K. Johnson, A. Kiriy, W. T. S. Huck and M. Sommer, *Macromolecules*, 2011, **44**, 9164–9172.

51 R. Tkachov, V. Senkovskyy, H. Komber, J.-U. Sommer and A. Kiriy, *J. Am. Chem. Soc.*, 2010, **132**, 7803–7810.

52 E. L. Lanni and A. J. McNeil, *J. Am. Chem. Soc.*, 2009, **131**, 16573–16579.

53 B. C. Achord and J. W. Rawlins, *Macromolecules*, 2009, **42**, 8634–8639.

54 R. Miyakoshi, A. Yokoyama and T. Yokozawa, *J. Am. Chem. Soc.*, 2005, **127**, 17542–17547.

55 M. C. Iovu, E. E. Sheina, R. R. Gil and R. D. McCullough, *Macromolecules*, 2005, **38**, 8649–8656.

56 A. N. Desnoyer, W. Chiu, C. Cheung, B. O. Patrick and J. A. Love, *Chem. Commun.*, 2017, **53**, 12442–12445.

57 G. Erker, U. Dorf, P. Czisch and J. L. Peterson, *Organometallics*, 1986, **5**, 668–676.

58 G. Erker, U. Dorf, J. L. Atwood and W. E. Hunter, *J. Am. Chem. Soc.*, 1986, **108**, 2251–2257.

59 F. R. Askham, K. M. Carroll, S. J. Alexander, A. L. Rheingold and B. S. Haggerty, *Organometallics*, 1993, **12**, 4810–4815.

60 J. E. Hill, P. E. Fanwick and I. P. Rothwell, *Organometallics*, 1992, **11**, 1771–1773.

61 G. Fachinetti, C. Biran, C. Floriani, A. Chiesi-Villa and C. Guastini, *J. Am. Chem. Soc.*, 1978, **100**, 1921–1922.

62 L. Li, K. E. Kristian, A. Han, J. R. Norton and W. Sattler, *Organometallics*, 2012, **31**, 8218–8224.

63 P. T. Wolczanski, *Organometallics*, 2017, **36**, 622–631.

64 G. Parkin, *J. Chem. Educ.*, 2006, **83**, 791.

65 M. L. H. Green and G. Parkin, *J. Chem. Educ.*, 2014, **91**, 807–816.

66 L. Yang, D. R. Powell and R. P. Houser, *Dalt. Trans.*, 2007, 955–964.

67 M. Benedetti, C. R. Barone, D. Antonucci, V. M. Vecchio, A. Ienco, L. Maresca, G. Natile and F. P. Fanizzi, *Dalt. Trans.*, 2012, **41**, 3014.

68 Wadepohl CCDC private communication.

69 B. de Bruin, M. J. Boerakker, J. A. W. Verhagen, R. de Gelder, J. M. M. Smits and A. W. Gal, *Chem. - A Eur. J.*, 2000, **6**, 298–312.

70 L. E. Doyle, W. E. Piers, J. Borau-Garcia, M. J. Sgro and D. M. Spasyuk, *Chem. Sci.*, 2016, **7**, 921–931.

71 L. E. Doyle, W. E. Piers and J. Borau-Garcia, *J. Am. Chem. Soc.*, 2015, **137**, 2187–2190.

72 M. Bühl, M. Håkansson, A. H. Mahmoudkhani and L. Öhrström, *Organometallics*, 2000, **19**, 5589–5596.

73 J. J. Garcia and W. D. Jones, *Organometallics*, 2000, **19**, 5544–5545.

74 J. J. Garcia, N. M. Brunkan and W. D. Jones, *J. Am. Chem. Soc.*, 2002, **124**, 9547–9555.

75 T. A. Ateşin, T. Li, S. Lachaize, W. W. Brennessel, J. J. García and W. D. Jones, *J. Am. Chem. Soc.*, 2007, **129**, 7562–7569.

76 D. J. Mindiola, R. Waterman, D. M. Jenkins and G. L. Hillhouse, *Inorganica Chim. Acta*, 2003, **345**, 299–308.

77 R. Waterman and G. L. Hillhouse, *J. Am. Chem. Soc.*, 2008, **130**, 12628–12629.

78 J. J. Curley, K. D. Kitiachvili, R. Waterman and G. L. Hillhouse, *Organometallics*, 2009, **28**, 2568–2571.

79 D. J. Mindiola, R. Waterman, V. M. Iluc, T. R. Cundari and G. L. Hillhouse, *Inorg. Chem.*, 2014, **53**, 13227–13238.

80 P. N. Plessow, L. Weigel, R. Lindner, A. Schäfer, F. Rominger, M. Limbach and P. Hofmann, *Organometallics*, 2013, **32**, 3327–3338.

81 R. Doi, K. Kikushima, M. Ohashi and S. Ogoshi, *J. Am. Chem. Soc.*, 2015, **137**, 3276–3282.

82 J. E. Penner-Hahn, in *Comprehensive coordination chemistry II From Biology to Nanotechnology*, eds. A. B. P. Lever, J. A. McCleverty and T. J. Meyer, Elsevier Pergamon, 2nd Editio., 2005, vol. 2, pp. 159–186.

83 N. C. Tomson, K. D. Williams, X. Dai, S. Sproules, S. DeBeer, T. H. Warren and K. Wieghardt, *Chem. Sci.*, 2015, **6**, 2474–2487.

84 T. E. Westre, P. Kennepohl, J. G. DeWitt, B. Hedman, K. O. Hodgson and E. I. Solomon, *J. Am. Chem. Soc.*, 1997, **119**, 6297–6314.

85 S. N. MacMillan and K. M. Lancaster, *ACS Catal.*, 2017, **7**, 1776–1791.

86 J. L. DuBois, P. Mukherjee, T. D. P. Stack, B. Hedman, E. I. Solomon and K. O. Hodgson, *J. Am. Chem. Soc.*, 2000, **122**, 5775–5787.

87 J. Kowalska and S. DeBeer, *Biochim. Biophys. Acta - Mol. Cell Res.*, 2015, **1853**, 1406–1415.

88 T. Yamamoto, *X-Ray Spectrom.*, 2008, 37, 572–584.

89 A. Kuzmin, N. Mironova, J. Purans and A. Rodionov, *J. Phys. Condens. Matter*, 1995, **7**, 9357–9368.

90 A. Corrias, G. Mountjoy, G. Piccaluga and S. Solinas, *J. Phys. Chem. B*, 1999, **103**, 10081–10086.

91 A. Rougier, C. Delmas and A. V. Chadwick, *Solid State Commun.*, 1995, **94**, 123–127.

92 I. J. Pickering, G. N. George, J. T. Lewandowski and A. J. Jacobson, *J. Am. Chem. Soc.*, 1993, **115**, 4137–4144.

93 A. N. Mansour and C. A. Melendres, *J. Phys. Chem. A*, 1998, **102**, 65–81.

94 C. Gougoussis, M. Calandra, A. Seitsonen, C. Brouder, A. Shukla and F. Mauri, , DOI:10.1103/PhysRevB.79.045118.

95 J. Cho, R. Sarangi, J. Annaraj, S. Y. Kim, M. Kubo, T. Ogura, E. I. Solomon and W. Nam, *Nat. Chem.*, 2009, **1**, 568–572.

96 K.-R. Pörschke, C. Pluta, B. Proft, F. Lutz and C. Krüger, *Zeitschrift für Naturforsch. B*, , DOI:10.1515/znb-1993-0511.

97 M. Schultz, P.-N. Plessow, F. Rominger and L. Weigel, *Acta Crystallogr. Sect. C Cryst. Struct. Commun.*, 2013, **69**, 1437–1447.

98 M. Joost, L. Estévez, S. Mallet-Ladeira, K. Miqueu, A. Amgoune and D. Bourissou, *Angew. Chemie Int. Ed.*, 2014, **53**, 14512–14516.

99 S. Dapprich and G. Frenking, *J. Phys. Chem.*, 1995, **99**, 9352–9362.

100 A. E. Reed, L. a Curtiss and F. Weinhold, *Chem. Rev. (Washington, DC, United States)*, 1988, **88**, 899–926.

101 L. J. Farrugia, C. Evans, D. Lentz and M. Roemer, , DOI:10.1021/ja808303j.

102 R. D. Bertrand, F. B. Ogilvie and J. G. Verkade, *J. Am. Chem. Soc.*, 1970, **92**, 1908–1915.

103 E. D. Glendening and F. Weinhold, *J. Comput. Chem.*, 1998, **19**, 593–609.

104 E. D. Glendening and F. Weinhold, *J. Comput. Chem.*, 1998, **19**, 610–627.

105 E. D. Glendening, J. K. Badenhoop and F. Weinhold, *J. Comput. Chem.*, 1998, **19**, 628–646.

106 J. T. Groves, *Nat. Chem.*, 2014, **6**, 89–91.

107 I. Bach, R. Goddard, C. Kopiske, K. Seevogel and K.-R. Pörschke, *Organometallics*, 1999, **18**, 10–20.

108 W. He, B. O. Patrick and P. Kennepohl, η^2 bonded Nickel(0) thiophene π-complexes - identifying the missing link in catalyst transfer polymerization, https://chemrxiv.org/articles/_2_bonded_Nickel_0_thiophene_-complexes_-_identifying_the_missing_link_in_catalyst_transfer_polymerization/5758608, (accessed 17 January 2018).

109 I. Bach, K.-R. Pörschke, R. Goddard, C. Kopiske, C. Krüger, A. Rufińska and K. Seevogel, *Organometallics*, 1996, **15**, 4959–4966.

110 A. G. MacDiarmid, Ed., *Inorganic Syntheses*, John Wiley & Sons, Inc., Hoboken, NJ, USA, 1977, vol. 17.

111 S. M. Webb, *Phys. Scr.*, 2005, **T115**, 1011–1014.

112 B. Ravel and M. Newville, in *Journal of Synchrotron Radiation*, International Union of Crystallography, 2005, vol. 12, pp. 537–541.